



Design, synthesis, and biological evaluation studies of novel carboxylesterase 2 inhibitors for the treatment of irinotecan-induced delayed diarrhea



Zhongcheng Yang ^{a,1}, Zhijun Cao ^{a,b,c,1}, Wenxin Wang ^a, Ya Chen ^a, Wanqiu Huang ^{a,b,c,d}, Shixuan Jiao ^{a,b,c}, Siliang Chen ^a, Lianru Chen ^a, Yuxia Liu ^a, Jianming Mao ^a, Luyong Zhang ^{c,d,*}, Zheng Li ^{a,b,c,d,e,*}

^a School of Pharmacy, Guangdong Pharmaceutical University, Guangzhou 510006, PR China

^b Key Specialty of Clinical Pharmacy, The First Affiliated Hospital of Guangdong Pharmaceutical University, Guangzhou 510006, PR China

^c Key Laboratory of New Drug Discovery and Evaluation of the Guangdong Provincial Education Department, Guangdong Pharmaceutical University, Guangzhou 510006, PR China

^d Guangzhou Key Laboratory of Construction and Application of New Drug Screening Model Systems, Guangdong Pharmaceutical University, Guangzhou 510006, PR China

^e Guangdong Key Laboratory of Pharmaceutical Bioactive Substances, Guangdong Pharmaceutical University, Guangzhou 510006, PR China

ARTICLE INFO

Keywords:

Human carboxylesterase 2
Irinotecan
Delayed diarrhea
Molecular dynamics simulation
Molecular docking

ABSTRACT

Human carboxylesterase 2 (hCES2A), one of the most important serine hydrolases distributed in the small intestine and colon, plays a crucial role in the hydrolysis of various prodrugs and esters. Accumulating evidence has demonstrated that the inhibition of hCES2A effectively alleviate the side effects induced by some hCES2A-substrate drugs, including delayed diarrhea caused by the anticancer drug irinotecan. Nonetheless, there is a scarcity of selective and effective inhibitors that are suitable for irinotecan-induced delayed diarrhea. Following screening of the in-house library, the lead compound **01** was identified with potent inhibition on hCES2A, which was further optimized to obtain **LK-44** with potent inhibitory activity ($IC_{50} = 5.02 \pm 0.67 \mu\text{M}$) and high selectivity on hCES2A. Molecular docking and molecular dynamics simulations indicated that **LK-44** can formed stable hydrogen bonds with amino acids surrounding the active cavity of hCES2A. The results of inhibition kinetics studies unveiled that **LK-44** inhibited hCES2A-mediated FD hydrolysis in a mixed inhibition manner, with a K_i value of $5.28 \mu\text{M}$. Notably, **LK-44** exhibited low toxicity towards HepG2 cells according to the MTT assay. Importantly, *in vivo* studies showed that **LK-44** significantly reduced the side effects of irinotecan-induced diarrhea. These findings suggested that **LK-44** is a potent inhibitor of hCES2A with high selectivity against hCES1A, which has potential as a lead compound for the development of more effective hCES2A inhibitors to mitigate irinotecan-induced delayed diarrhea.

1. Introduction

Mammalian carboxylesterases (CES) belong to a vital member of the serine hydrolase superfamily (EC3.1.1.1), which are localized in the lumen of the endoplasmic reticulum. As one of the serine hydrolases, CES hydrolyzes a variety of endogenous and exogenous substances containing ester bonds by a catalytic Ser-His-Glu triad [1–3]. In the past 20 years, human carboxylesterase can be roughly divided into five

subtypes, of which human carboxylesterase 1A (hCES1A) and human carboxylesterase 2A (hCES2A) have received the most attention. The amino acid sequence homology between hCES1A and hCES2A is 47%. Furthermore, substrate selectivity and tissue distribution also show marked differences, highlighting distinct functional roles across the two subtypes [4–6]. In general, hCES1A is expressed mainly in the liver and tends to hydrolyze ester substrates which containing small alcohol groups and large acyl groups such as Enalapril, Oseltamivir, Clopidogrel

* Corresponding authors at: Key Laboratory of New Drug Discovery and Evaluation of the Guangdong Provincial Education Department, Guangdong Pharmaceutical University, Guangzhou 510006, PR China.

E-mail addresses: lyzhang@cpu.edu.cn (L. Zhang), lizhengdrug@gdpu.edu.cn (Z. Li).

¹ These authors made equal contributions to this work.

[7–9]. In contrast, hCES2A is primarily distributed in the intestine and colon, and its substrate specificity is the opposite of that of hCES1A. It mainly participates in the metabolism of alcohol groups and small acyl groups [10,11]. While the protein structure of hCES2A has not been characterized, several crystal structures of hCES1A have been published. These structures provide valuable insights into the functional mechanisms of protein, which is useful for the discovery and development of drugs targeting hCES2A [12–14].

In addition, hCES2A, as the main carboxylesterase in the intestine, plays a crucial role in the treatment of ester-based anticancer drugs. For example, CPT-11 (irinotecan) is widely used worldwide as a first-line cancer drug. After intravenous injection, irinotecan is rapidly metabolized into SN-38 by hCES2A, which exerted potent anticancer activity. However, excessive accumulation of SN-38 in the intestine and colon can cause severe delayed diarrhea, which, if not treated promptly, can be life-threatening for the patient [15–17]. Loperamide (LPA) is a commonly used medication in clinical settings to prevent or treat both acute and chronic diarrhea. It is known to alleviate the discomfort caused by diarrhea in the majority of patients. Although loperamide is used in clinical practice, it has been found to have insufficient inhibitory activity and selectivity to fully meet the requirements for effective treatment. Significantly, the adverse effects of loperamide, including constipation, skin allergy, somnolence, and nausea, have restricted its clinical application [18]. And beyond that, there are few drugs that can be combined with irinotecan to reduce diarrhea.

While numerous natural and synthetic compounds have been documented (Fig. 1) [19–24], the majority of them are bound through covalent bonds or contain an excessive number of phenolic hydroxyl groups, resulting in unfavorable pharmacokinetics and properties for drug development. In addition, certain phenolic compounds may interact with other drugs within the body, potentially compromising their efficacy or inducing toxic side effects [25,26]. Thus, there is still room for further development of hCES2A inhibitors to treat irinotecan-induced delayed diarrhea. Currently, research and development efforts are mostly focused on *in vitro* characterization, and only a few compounds have been thoroughly examined in the irinotecan-induced delayed diarrhea model. Thus, the objective of this study was to discover a potent and selective inhibitor of hCES2A and investigate the inhibitor *in vivo* properties for the improvement of irinotecan-induced delayed diarrhea treatment (Fig. 2). Herein, we performed a high-throughput screening in our in-house library, and led to the discovery

of lead compound **01** ($IC_{50} = 46.95 \pm 0.80 \mu M$) with novel skeleton. Based on the molecular modeling study of hCES2A and lead compound **01**, a series of compounds were designed to explore the structure–activity relationship of the present series, which providing the optimal compound **LK-44** ($IC_{50} = 5.02 \pm 0.67 \mu M$). Moreover, **LK-44** significantly improved diarrhea induced by irinotecan and that the therapeutic effect was superior to that of loperamide.

2. Results and discussion

2.1. Chemistry

The preparative methods for compounds **1–19**, **22–27**, **29**, and **37–39** were outlined in detail in Scheme 1. The alkylation of **1a** using alkyl halide via the standard Williamson ether synthesis method yielded intermediates **2a–j**, which were subsequently converted to compounds **1–19**, **22–27**, **29**, and **37–39** exclusively in the Z-configuration under alkali conditions. Compounds **20–21** and **28** were synthesized according to the procedure outlined in Scheme 2. Briefly, halogenated alkyl groups were condensed with **3a** and **5a** at $45^\circ C$ to form **6a–c**, which were subsequently converted to **20–21** and **28**. The compounds **30–32** were synthesized as shown in Scheme 3. The amide derivative **30** was obtained by condensation reaction of **29** with acetyl chloride under alkaline conditions. In the presence of piperidine, compound **29** was condensed with benzenesulfonyl chloride or TsCl for 24 h to give **31–32**. Due to a significant reduction in yield when **2c** was reacted with **7a–b**, improvements were made by preserving the bare phenolic hydroxyl group of **1c** during binding and subsequent condensation reactions with 1-bromopropane before hydrolysis, resulting in a better yield. The synthesis of compounds **33–34** was depicted in Scheme 4. Intermediate **1a** was created via Williamson ether synthesis to produce **7a–b**, which was subsequently condensed under alkaline conditions, resulting in intermediate **8a–b**. Hydrolysis of intermediates **8a–b** with 1-bromopropane condensation yielded the desired compounds (**33–34**). Compounds **35–36** and **40–45** were obtained as described in Scheme 5. Alkylation of **3a**, **3c–e**, **5a** with alkyl halide under the reaction of Williamson ether synthesis supplied intermediates **10a–h**, which were converted into **11a–h** under alkali conditions. The alkylation of **11a–h** with 1-bromopropane using potassium carbonate as an acid binding agent, followed by hydrolysis under basic condition resulted in the formation of compounds **35–36** and **40–45**.

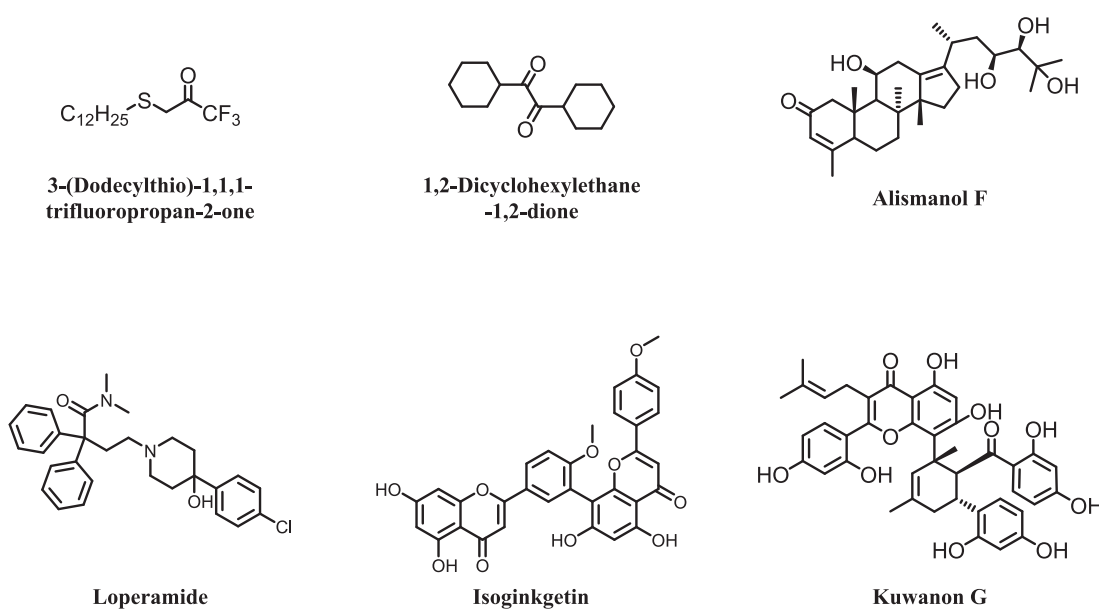


Fig. 1. Inhibitors of hCES2A.

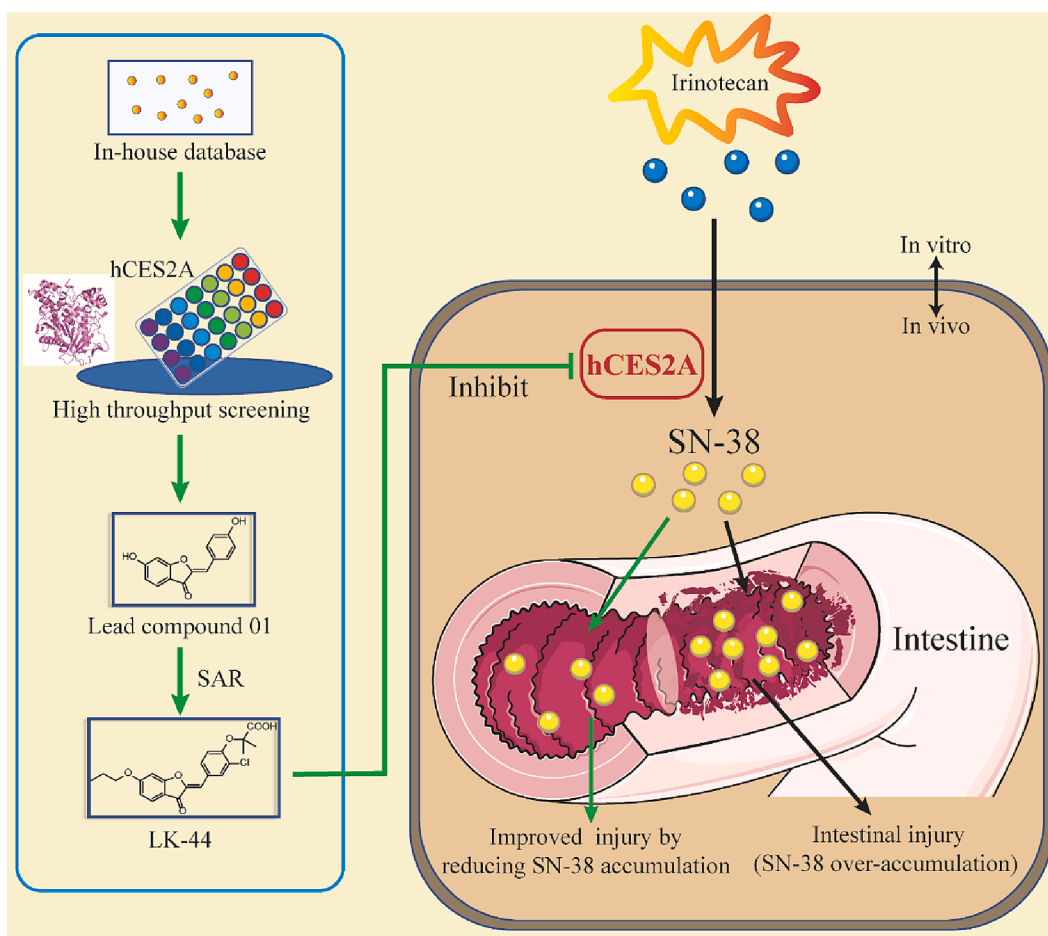


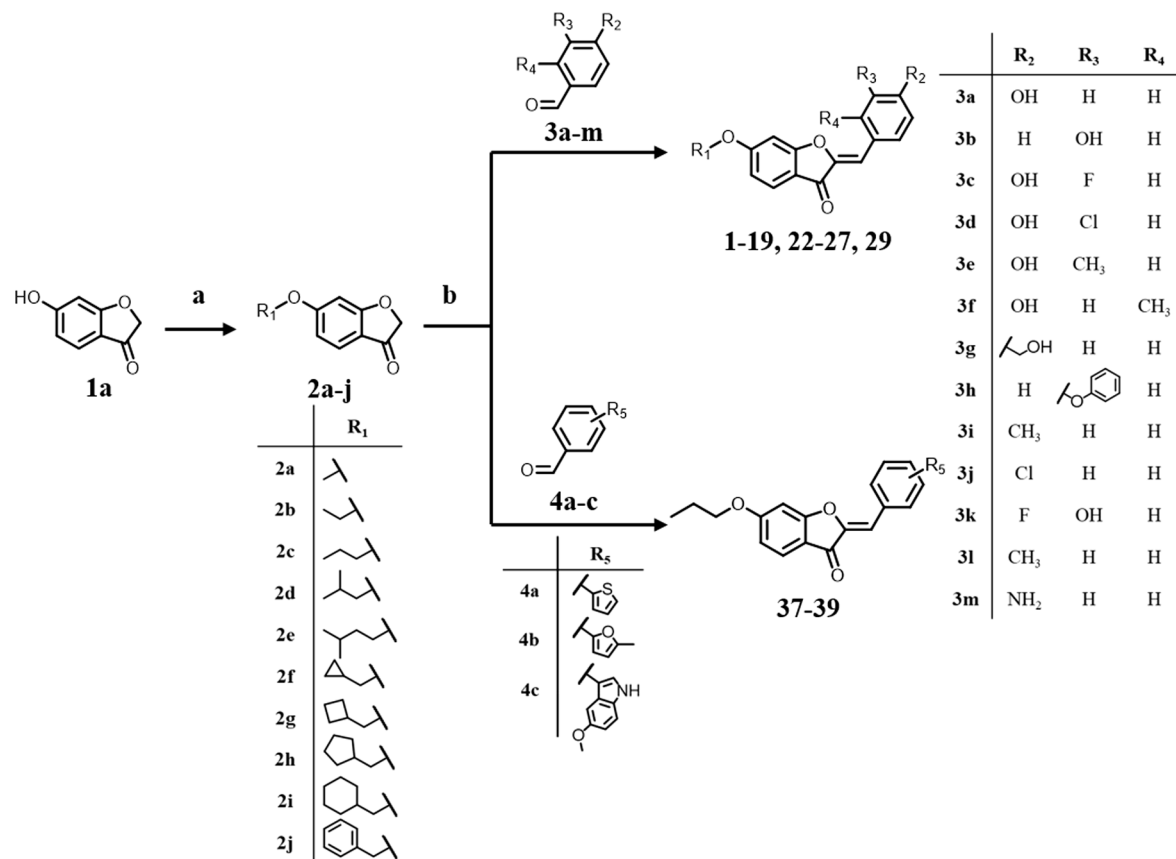
Fig. 2. The process of obtaining lead compound and the mechanism of irinotecan induced delayed diarrhea.

2.2. SAR study

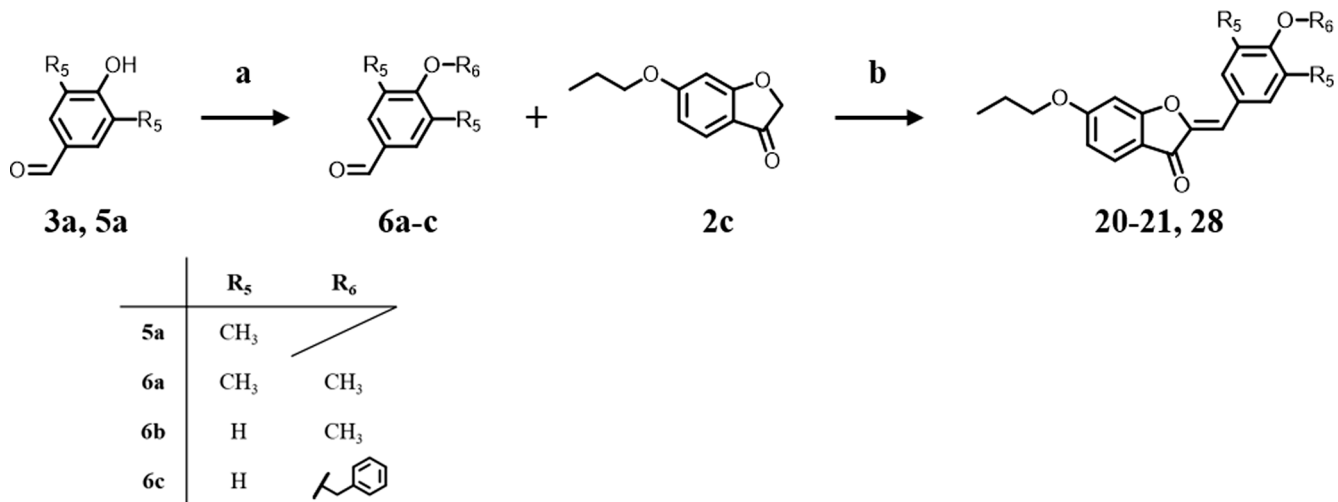
In order to explore novel hCES2A inhibitors, we performed a high-throughput screening in our in-house library, which resulted in the discovery of lead compound **01** ($IC_{50} = 46.95 \pm 0.80 \mu M$). Moreover, the molecular modeling study of hCES2A and lead compound **01** was performed to better understand its binding mode. As shown in Fig. 3A–B, compound **01** fitted well with the binding pocket of hCES2A by forming multiple hydrogen bonds with I350, L349, and S228. However, there was still hydrophobic cavity around the hydroxyl group at benzofuran-3 (2H)-one (red circle mark in Fig. 3B), which was a potential site suitable for further modification by introducing hydrophobic substituents. Based on these molecular modeling results, a series of compounds were designed to explore the structure–activity relationship of the present series. As depicted in Table 1, the compounds with varied hydrophobic groups on the hydroxyl of compound **01** exhibited varying degrees of inhibition towards hCES2A. Among the chained alkanes (**1–5**), *n*-propyl (**3**) and isobutyl group (**4**) demonstrated the best inhibition. Compounds **6–9**, which contain cyclic groups, were also found to improve inhibition, although the extent of inhibition decreased as the ring size increased. This could be due to restrictions in the hydrophobic cavity available at this position. Furthermore, it was demonstrated that the flexible alkane chain was more potent in inhibiting hCES2A than the cycloalkyl chain. In fact, upon substitution of cyclohexane (**9**) with a benzene ring (**10**), the inhibitory activity showed a steep decline. In short, the results in Table 1 clarified that hydrophobic groups could be introduced into the head of the lead compound **01**. Notably, compounds **3** and **4** displayed the highest hCES2A inhibition, thus piquing our interest for additional structural studies.

Further studies showed that the introduction of halogens (**12–13, 16, 18**) in the *meta*-position of benzene rings at the tail of compounds **3** and **4** improved the inhibitory activity, but it is in-tolerated if the hydroxyl group was changed to the *meta*-position (**11** and **15**). The decreased inhibitory activity observed upon substituting the methyl group (**14** and **17**) suggested that the placement of small electron-withdrawing groups (such as halogens) in this position may be more favorable for matching the hCES2A pocket. Compound **19** was designed based on the assumption that the dihedral angle of benzene ring might affect the activity. Indeed, the activity of the *ortho*-methyl group decreased sharply, suggesting that *ortho*-substitution was in-tolerated in this area. In conclusion, *n*-propyl group exhibited the best inhibitory activity in this series, so we chose *n*-propyl group as the best substituent in the head of benzofuran-3(2H)-one.

In order to investigate the influence of the phenolic hydroxyl group on hCES2A inhibitory activity, we directed our attention towards the structure–activity relationship at the tail of the benzene ring (Table 2). Notably, compounds **20–22** displayed considerably lower inhibitory activities compared to compound **3** when the hydroxyl group was replaced with methoxyl or benzyl alcohol. To further explore whether larger substituents in this area could form hydrophobic interactions, compounds **23** and **28** were designed. However, none of these compounds demonstrated significant inhibitory effects. Notably, the introduction of a methyl group (**24**), halogens (**25** and **26**), and a trifluoromethyl group (**27**) onto the benzene ring proved intolerable, underscoring the critical role of the hydroxyl group in the inhibitory activity. Moreover, the hydroxyl group was also replaced by amino group (**29**), which is also a hydrogen bond donor. Strangely, compound **29** showed no improvement in inhibitory activity and even exhibited



Scheme 1. Synthesis of target compounds **1-19**, **22-27**, **29** and **37-39**. Reagents and conditions: (a) Alkyl halide, K_2CO_3 , acetonitrile, KI , $45\text{ }^\circ C$, 12 h; (b) $DMF/EtOH = 1:1$, KOH , r.t., 6–18 h, 45–71%.

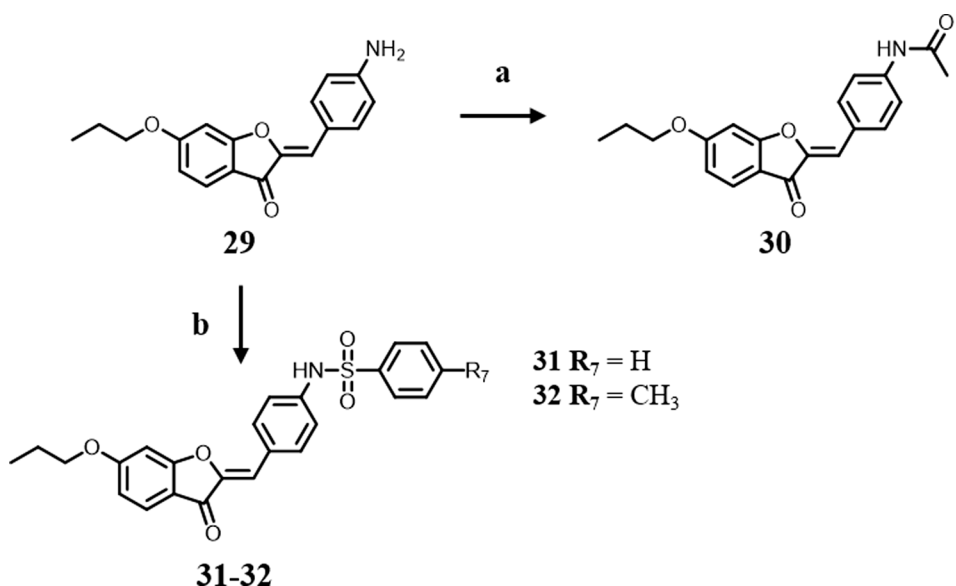


Scheme 2. Synthesis of target compounds **20-21** and **28**. Reagents and conditions: (a) Alkyl halide, K_2CO_3 , acetonitrile, KI , $45\text{ }^\circ C$, 10–12 h; (b) $DMF/EtOH = 1:1$, KOH , r.t., 6–12 h, 49–61%.

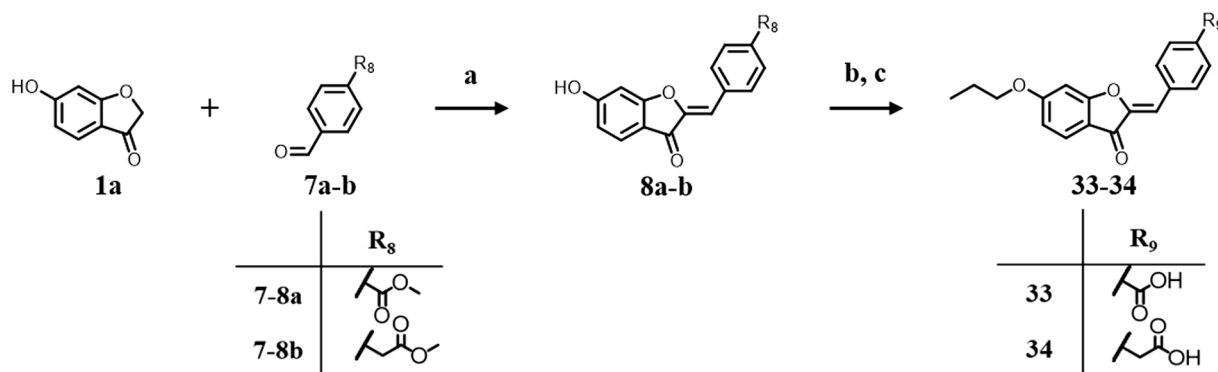
worse inhibitory effects than compound **3**. This could be due to a misfit between the basic amino group and the binding pocket. Furthermore, we attempted to reduce the basicity of the amino group by condensing it into an amide form. Compounds **30–32** suggested that the reduction of basicity was favorable for improving the inhibitory activity (**30**), while enhancing rigidity resulted in decreased inhibitory activity (**31–32**). Notably, the introduction of distinct carboxyl moieties (**33–36**) at this position was well-tolerated. Compound **35**, which featured a phenoxyacetic acid moiety, demonstrated the highest inhibitory activity among

these carboxyl moieties. In further studies, it was found that benzene rings were substituted with heterocyclic rings (**37–39**). However, despite modifications to the structure, the inhibitory activity against hCES2A remained low. Therefore, it is clear that the benzene ring at the tail of the structure is beneficial.

According to the mono-substitution SAR, we made some combinations and designed compounds containing halogens (or methyl) and carboxylic acids (**40–45**). As shown in Table 3, the introduction of a single methyl group (**40**: $16.13\text{ }\mu M$) into phenoxyacetic acid moiety



Scheme 3. Synthesis of target compounds 30–32. Reagents and conditions: (a) Acetyl chloride, triethylamine, DMAP, DCM, 0 °C, 5 h; (b) TsCl or benzenesulfonyl chloride, pyridine, DCM, 0 °C-r.t., 24 h, 50–56%.



Scheme 4. Synthesis of target compounds 33 and 34. Reagents and conditions: (a) DMF/ EtOH = 1:1, KOH, r.t., 8–10 h; (b) Alkyl halide, K_2CO_3 , acetonitrile, KI, 45 °C, 12 h; (c) $\text{LiOH}\cdot\text{H}_2\text{O}$, THF/MeOH/ H_2O = 2:3:1, r.t., 4 h, 55–67%.

slightly increased the inhibitory activity, and the introduction of dimethyl group (41: 15.12 μM) further increased the activity. Meanwhile, methyl groups (42: 18.25 μM) were introduced into the *meta*-position of the benzene ring, and the halogen analogs (43: 9.98 μM ; 44: 5.02 μM) revealed better inhibitory activity than that of 41. Among them, compound 44 (LK-44) displayed the best inhibitory activity on hCES2A in this series.

Prior to further experiments, we conducted an MTT assay on LK-44 (Fig. S1). According to the results, the cell inhibition rate gradually increased with increasing concentrations of LK-44. Notably, the cell inhibition rate remained relatively low even at the dosage of 20 μM , which was apparently higher than the IC_{50} value of LK-44, indicating that LK-44 had relatively low toxicity in the pharmaceutical dosage.

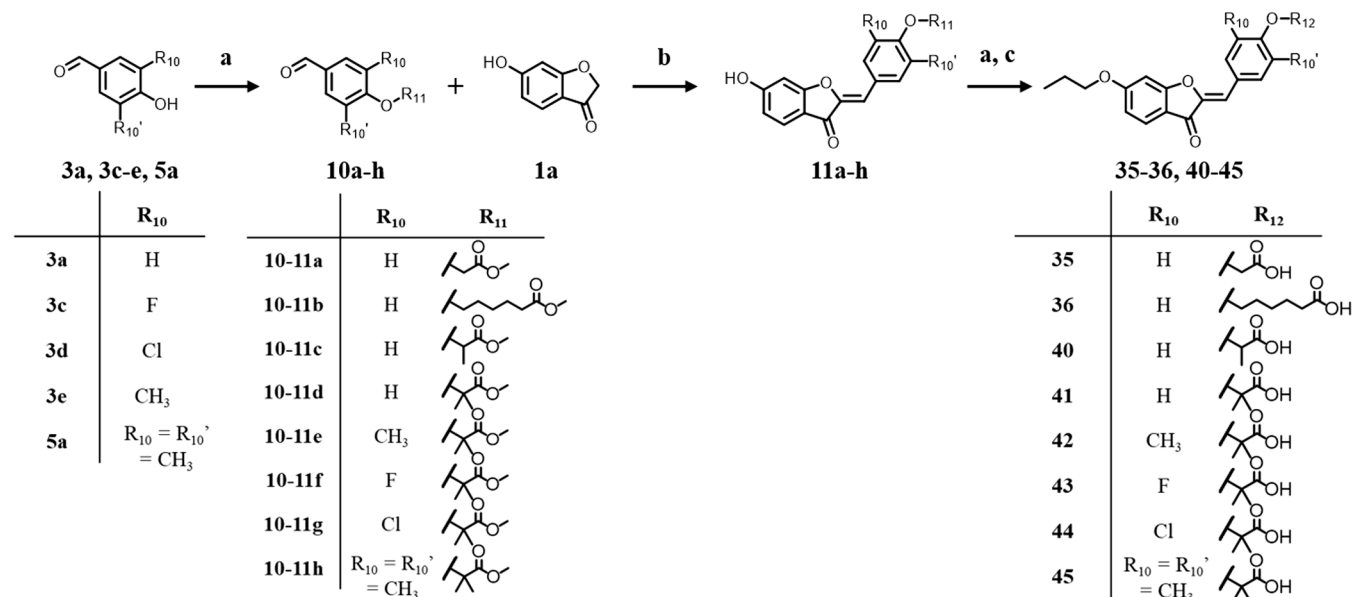
In summary, the structure–activity relationship could be summarized as follows: the introduction of *n*-propyl group at the head of compound 01 significantly enhanced the inhibitory activity, and the inclusion of a flexible carboxylic acid chain in the tail of the compound also improves the inhibitory activity. Additionally, the presence of a chlorine atom between the phenyl rings in the tail slightly enhanced the inhibitory activity of compounds. These results not only help us to better understand the characteristics of hCES2A inhibitors, but also provide guidance for the design of more selective and active new molecules.

2.3. Selectivity of LK-44 towards hCES1A

Due to the high similarity between hCES1A and hCES2A as members of the serine hydrolase superfamily, it was crucial to assess the selectivity of LK-44 to avoid off-target toxicity of hCES1A. Therefore, *D*-Luciferin methyl ester (DME), a reported specific optical substrate, was utilized to screen the inhibitory activity of LK-44 on hCES1A [27]. As shown in Table 4, LK-44 is a potent hCES2A inhibitor with a high selectivity against hCES1A (> 100 μM).

2.4. Inhibition kinetics of LK-44 against hCES2A

Encouraged by these encouraging results, we sought to delve deeper into the inhibitory mechanism of LK-44 on hCES2A by conducting inhibition kinetic analysis. Time-dependent inhibition assays (3 min and 33 min) were conducted to determine the type of inhibition caused by LK-44. As shown in Fig. 4B, it was found that the inhibition curves at 3 min and 33 min were not significantly different after appropriately extending the pre-incubation time. This indicated that the effect of LK-44 on hCES2A did not change with time. Therefore, LK-44 is a reversible inhibitor of hCES2A. Based on this result, we designed experiments in which LK-44 inhibited hCES2A-mediated FD hydrolysis of fluorescent probe substrates. As demonstrated in Fig. 4C-E, at various



Scheme 5. Synthesis of target compounds 35–36, 40–45. Reagents and conditions: (a) Alkyl halide, K₂CO₃, acetonitrile, KI, 45 °C, 12–18 h; (b) DMF/EtOH = 1:1, KOH, r.t., 10–12 h; (c) LiOH-H₂O, THF/MeOH/H₂O = 2:3:1, r.t., 4 h, 45–60%.

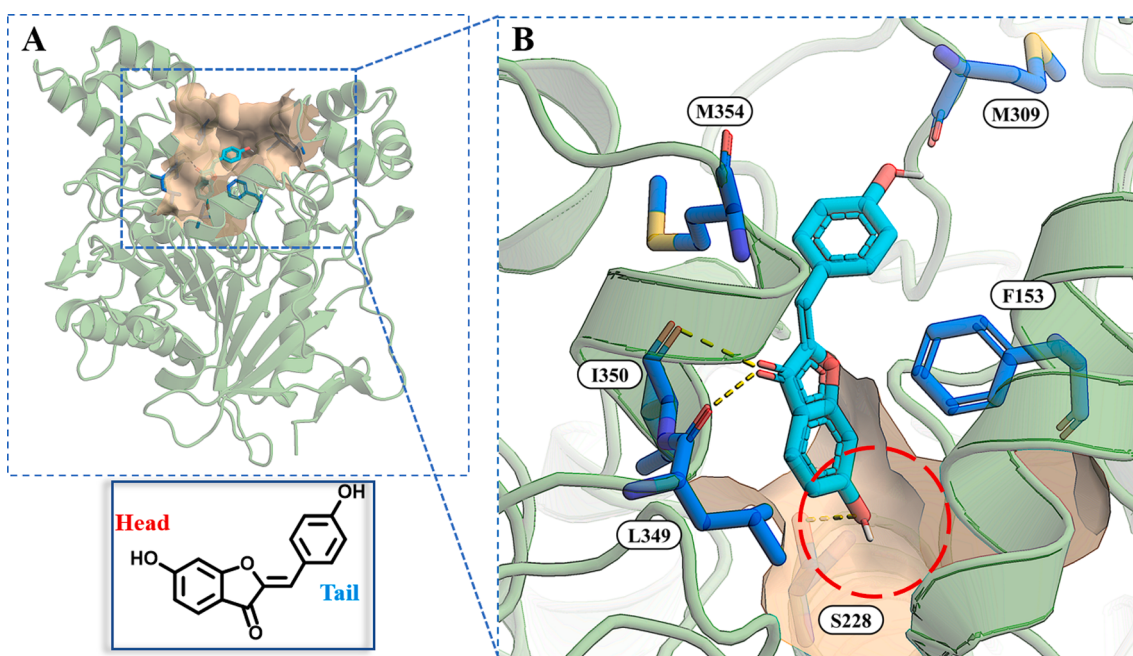


Fig. 3. The docking study of lead compound 01. (A) Panoramic view of the docking results of lead compound 01 and hCES2A; (B) Diagram of interaction between lead compound 01 and hCES2A.

concentrations of LK-44, the Lineweaver-Burk plot revealed that LK-44 inhibited hCES2A-mediated FD hydrolysis in a mixed manner, with a measured *K_i* value of 5.28 μM. Overall, these results suggested that LK-44 functions as a mixed reversible inhibitor of hCES2A.

2.5. Docking study

To better understand the activity and selectivity of LK-44 towards hCES1A and hCES2A, a docking study was conducted utilizing hCES1A (1MX1) and the structure of hCES2A obtained via homologous modeling. Initially, LK-44 was docked into the structure of hCES2A (Fig. 5A-B), revealing that both LK-44 and the lead compound 01 formed three hydrogen bonds with I350, L349, and S228 (Figs. 3B and

5B). Furthermore, the carboxyl group of LK-44 was found to establish an additional hydrogen bonding interaction with M309, and the propoxy group was noted to fit well into the cavity located at the pocket's bottom. To further investigate the conformation of LK-44, we merged the docking results of LK-44 and the lead compound 01 together (Fig. 5C). To our surprise, the benzofuran-3(2H)-one structure of compounds 44 and 01 demonstrated significant overlap, generating an angle between the two benzene rings. The possible reason was that the chlorine in the benzene ring of LK-44 reached into the small hydrophobic pocket formed by G261 and L262, fixing the benzene ring conformation. In addition, the two methyl groups at the tail of LK-44 occupied hydrophobic positions, allowing carboxyl group to exert better binding interaction with M309. However, when LK-44 was docked into the

Table 1 The inhibitory effect of compounds 1–19 against hCES2A.

Compds	R ₁	R ₂	R ₃	R ₄	Inhibition ratio (%) ^a		
					2 μM	20 μM	40 μM
Loperamide					29.49	67.94	71.51
01	H	OH	H	H	-5.44	18.37	41.76
1	✗	OH	H	H	1.25	20.59	43.59
2	✗	OH	H	H	3.58	21.96	48.52
3	✗	OH	H	H	11.62	27.22	60.57
4	✗	OH	H	H	10.08	25.65	59.83
5	✗	OH	H	H	4.73	15.11	47.93
6	✗	OH	H	H	5.18	21.13	52.89
7	✗	OH	H	H	4.93	20.96	46.43
8	✗	OH	H	H	6.52	17.96	45.95
9	✗	OH	H	H	2.79	13.42	39.88
10	✗	OH	H	H	-1.4	8.44	23.06
11	✗	H	OH	H	7.58	17.61	47.04
12	✗	OH	F	H	13.03	27.16	62.68
13	✗	OH	Cl	H	15.75	29.51	65.07
14	✗	OH	CH ₃	H	8.06	23.26	55.03
15	✗	H	OH	H	7.72	14.24	45.29
16	✗	OH	Cl	H	12.81	28.13	64.69
17	✗	OH	CH ₃	H	10.14	26.16	58.97
18	✗	OH	F	H	11.24	25.95	62.84
19	✗	OH	H	CH ₃	3.59	10.13	37.59

^a Inhibition ratio values were expressed as mean of the triplicate assays.

structure of hCES1A (1MX1) (Fig. 5D), it was found that the docking result of LK-44 and hCES1A was very poor. It was supposed that the chlorine atom in the benzene ring occupied the polar catalytic region, causing the carboxyl group to extend into the hydrophobic cavity of L255 and L318. The reduced binding ability of LK-44 due to these negative factors was consistent with its high selectivity against hCES1A.

2.6. Molecular dynamics simulation of hCES2A

To investigate the binding stability between hCES2A and the ligand, 50 ns molecular dynamics simulations were performed using the best docking pose. The dynamic stability and structural changes of the complex systems were analyzed by the examination of root-mean-square deviation (RMSD) of the protein backbone. As demonstrated in Fig. 6A, we conducted a simulation system for a total of 50 ns, and it stabilized around 5 ns with the RMSD value of the composite system fluctuating between 0.55 nm. These results suggested that LK-44 can be stably bound in the active pocket of hCES2A. To evaluate the flexibility of protein residues, we calculated the root-mean-square fluctuation (RMSF) of hCES2A and the complex. As depicted in Fig. 6B, both systems exhibited the same fluctuation pattern, with most residues displaying RMSF values of <0.2 nm, which indicated a relatively stable structure for these residues. Compared with hCES2A, residues E76-F81, A121-V123 and N418-P422 of the complex showed lower RMSF values than the free enzyme after removing the fluctuating effect of the protein. Notably, E76-F81 and A121-V123 were located in the active pocket (Fig. 6C),

which suggested that molecular interactions between the ligand bound in the pocket and the surrounding amino acids had stabilized the conformation of these amino acids.

Furthermore, to investigate the key residues involved in ligand binding in the complex, residues located within 8 Å of the ligand were selected, and the total binding free energy was calculated and decomposed into the contribution of individual residues (Fig. 6D). Residues with absolute decomposition energies exceeding 1.0 kcal/mol were deemed significant. Notably, the hydrophobic amino acids A150, V152, L262, M309, P311, and M354 were found to play a crucial role in the system, indicating that hydrophobic interactions played a dominant role in the binding of the protein and ligand. Analysis of the previous docking results revealed that M309 formed a hydrogen bond interaction with LK-44. Due to the fact that the ligand and the protein were in motion during the whole process of molecular dynamics simulation, the benzene ring of the ligand tail might form S-π conjugation with M354. These findings suggested that the aforementioned residues were critical in mediating the binding of LK-44 to hCES2A. Notably, hydrophilic amino acids such as S228 also made significant contributions, likely due to their role in the hydrolysis of esters as one of the catalytic triplex, and in stabilizing the conformation of inhibitors when they entered the pocket. These results have provided a more comprehensive understanding of the binding mode between hCES2A and inhibitors. Therefore, when designing hCES2A inhibitors, it is crucial to pay close attention to the interaction between the ligands and these key amino acids.

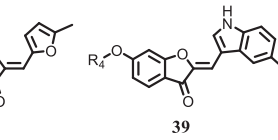
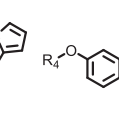
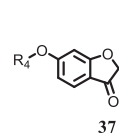
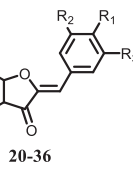
2.7. Effects of LK-44 on irinotecan-induced delayed diarrhea

To examine the therapeutic effect of LK-44 in irinotecan-induced delayed diarrhea, we conducted a 10-day animal experiment (Fig. 7A). In this study, LPA was selected as a positive control. The tested compound was administered via intragastric administration for 10 consecutive days, while irinotecan was injected intraperitoneally on days 4–7 to induce delayed diarrhea. As illustrated in Fig. 7B, the body weight of mice in the LPA group began to gradually decline, possibly due to the inhibition of intestinal smooth muscle contraction by LPA, leading to reduced intestinal peristalsis and slowing down the speed of digestion and metabolism, ultimately resulting in reduced food intake and weight loss. Weight loss was observed 24 h after irinotecan administration in the model group, as well as in the groups treated with LPA and LK-44. By day 8, the number of mice in the model and LPA treated groups had decreased due to death (Fig. 7C), and all groups exhibited diarrhea and hematochezia. Diarrhea was particularly severe in the model and LPA treated groups, with watery or bloody stools observed. According to the standard of Disease Activity Index (DAI), the scores of diarrhea, occult blood and weight loss of mice in the model group were significantly higher than those in the NC group, indicating that the diarrhea model was successfully implemented. The results in Fig. 7D-G indicated that the LK-44 treated group had significantly lower scores of diarrhea and occult blood compared to the model group and LPA treated group. Additionally, the DAI index reflected that LK-44 had a stronger effect in the diarrhea model than LPA. Further analysis of blood indexes showed that the levels of aspartate aminotransferase (AST), total bilirubin (TBIL) and blood urea nitrogen (BUN) were significantly increased in the model group compared to the control group (Fig. 7H-J). This suggests that irinotecan-induced delayed diarrhea not only affects the intestinal tract, but also causes liver and kidney damage due to its metabolism. Administration of LPA or LK-44 resulted in a significant reduction in plasma levels of AST, TBIL, and BUN. Furthermore, LK-44 demonstrated a capacity to maintain normal levels of uric acid (UA), alkaline phosphatase (ALP), and Alanine aminotransferase (ALT) (Fig. 7K-M), suggesting a protective effect on the liver.

In this study, the levels of IL-1β and IL-6 were significantly increased in the model group (Fig. 8A-C). This was due to delayed diarrhea caused by the excessive accumulation of SN-38, a metabolite of irinotecan, which damaged the intestinal mucosa and triggered high expression of

Table 2

The inhibitory effect of co-

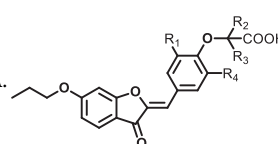


Compds	R ₁	R ₂	R ₃	R ₄	Inhibition ratio (%) ^a		
					2 μM	20 μM	40 μM
01	OH	H	H	H	-5.44	18.37	41.76
20		H	H		5.86	12.62	38.87
21		CH ₃	CH ₃		8.73	9.58	37.73
22		H	H		1.09	5.07	35.13
23	H		H		-3.63	4.34	29.82
24	CH ₃	H	H		2.18	3.92	18.29
25	Cl	H	H		8.33	10.36	34.83
26	F	H	H		3.24	5.91	27.93
27	CF ₃	H	H		5.36	8.19	34.85
28		H	H		6.12	3.24	30.22
29	NH ₂	H	H		-2.98	3.44	27.93
30		H	H		4.35	13.16	40.01
31		H	H		2.63	9.74	28.87
32		H	H		3.01	8.95	30.83
33		H	H		6.91	23.47	55.15
34		H	H		13.41	30.27	61.16
35		H	H		20.62	38.71	70.54
36		H	H		17.19	18.45	69.58
37					3.97	5.82	27.11
38					6.25	8.99	32.87
39					4.52	7.02	26.93

^a Inhibition ratio values were expressed as mean of the triplicate assays.

Table 3

The inhibitory effect of co-



Compds	R ₁	R ₂	R ₃	R ₄	Inhibition ratio (%) ^a			IC ₅₀ (μM) ^b
					2 μM	20 μM	40 μM	
Loperamide					29.49	67.94	71.51	7.71 ± 0.29
01					-5.44	18.37	41.76	46.95 ± 0.80
40	H	CH ₃	H	H	16.13	59.57	72.48	16.13 ± 0.17
41	H	CH ₃	CH ₃	H	18.44	55.68	74.81	15.21 ± 0.15
42	CH ₃	CH ₃	CH ₃	H	12.75	52.91	71.17	18.25 ± 0.42
43	F	CH ₃	CH ₃	H	23.67	60.94	81.51	9.98 ± 0.34
44 (LK-44)	Cl	CH ₃	CH ₃	H	33.48	74.93	87.56	5.02 ± 0.67
45	CH ₃	CH ₃	CH ₃	CH ₃	17.23	49.61	64.26	19.50 ± 0.93

^a Inhibition ratio values were expressed as mean of the triplicate assays.

^b IC₅₀ values were expressed as mean \pm SD of the triplicate assays.

Table 4

The inhibitory activity of LK-44 on hCES1A and hCES2A.

Compds	IC ₅₀ for hCES2A (μM) ^a	IC ₅₀ for hCES1A (μM) ^a	Selectivity ^b
LK-44	5.02 ± 0.67	> 100	> 19.9
BNPP	N.D.	1.35 ± 0.37	—
LPA	7.71 ± 0.29	N.D.	—

N.D. means not detected.

^a IC₅₀ value were expressed as mean ± SD of the triplicate assays.^b Selectivity is calculated from IC₅₀ (for hCES1A)/IC₅₀ (for hCES2A).

inflammatory markers. The administration of LPA and LK-44 led to a significant reduction in the levels of pro-inflammatory cytokines IL-1β and IL-6, while maintaining TNF-α levels within the normal range (Fig. 8D-E). Furthermore, the inhibitory effect of LK-44 on hCES2A expression in the colon was evaluated. As shown in Fig. 8F, the model group showed a significant increase in hCES2A content, which was reduced in both treated groups. Notably, the LK-44 treated group demonstrated a lower hCES2A level than the LPA treated group. As depicted in Fig. 9A, analysis of colon tissue stained with hematoxylin and eosin (H&E) revealed that the NC group had an intact structure of the intestinal mucosa and epithelium in all layers. Goblet and crypt cells were preserved, and glandular organization was orderly with no evidence of ulceration. Conversely, the model group exhibited compromised tissue architecture, evidenced by thickened intestinal mucosa, decreased crypt density, inflammatory cell infiltration, and irregular glandular arrangement. Following treatment with LPA, colon damage and ulceration of glands were mitigated, although damage to crypt and goblet cells remained unchanged. In contrast, LK-44 treatment led to a decrease in the number of inflammatory cells and reduced swelling. Furthermore, compared to both the model and LPA groups, LK-44 treatment increased gland density in the colon and significantly reduced damage to crypt and goblet cells. Further histological score (Fig. 9B) demonstrated that the LK-44 treated group had significantly lower scores than both the model and LPA groups. In the NC group, the colon had a normal morphology with granular contents. In contrast, the model

group exhibited a bloody appearance of the colon with liquid contents (Fig. 9C-D). Colonic injury was improved in both the LPA and LK-44 treated groups, and the contents appeared granular. Notably, the colon contents in the LK-44 group did not bleed, and the length was within the normal range. These results suggest that LK-44 significantly improved diarrhea induced by irinotecan, and its therapeutic effect was superior to that of LPA.

3. Conclusion

The hCES2A plays a crucial role in the hydrolysis of irinotecan, and the inhibition of hCES2A effectively alleviated the side effects induced by irinotecan. However, there is a scarcity of selective and effective hCES2A inhibitors that are suitable for irinotecan-induced delayed diarrhea, and it is necessary to design novel selective and efficient hCES2A inhibitors. In this study, a high-throughput screening was performed in an in-house library, which led to the discovery of lead compound 01 (IC₅₀ = 46.95 ± 0.80 μM). Based on the results of molecular docking, a structure-based complementarity strategy was employed to improve the activity of the lead compound 01. Subsequently, a series of compound rigidities, acid-base properties, and other characteristics were explored to achieve the goal of enhancing activity, resulting in the development of the optimal compound LK-44 with potent inhibitory activity (IC₅₀ = 5.02 ± 0.67 μM) and high selectivity against hCES1A. Inhibition kinetics analysis revealed that LK-44 exhibited mixed inhibition against hCES2A-mediated FD hydrolysis. Molecular docking and dynamics simulations further demonstrated that LK-44 formed hydrogen bonds with key amino acid residues including S228, M309, L349, and I350, with M309 and M354 contributing the most to the binding energy within the binding pocket. In addition, LK-44 effectively alleviated intestinal injury induced by irinotecan and showed low toxicity in MTT assay. With these encouraging results, the novel compound LK-44 could be an excellent candidate for further development of hCES2A inhibitor to benefit the field of cancer therapy.

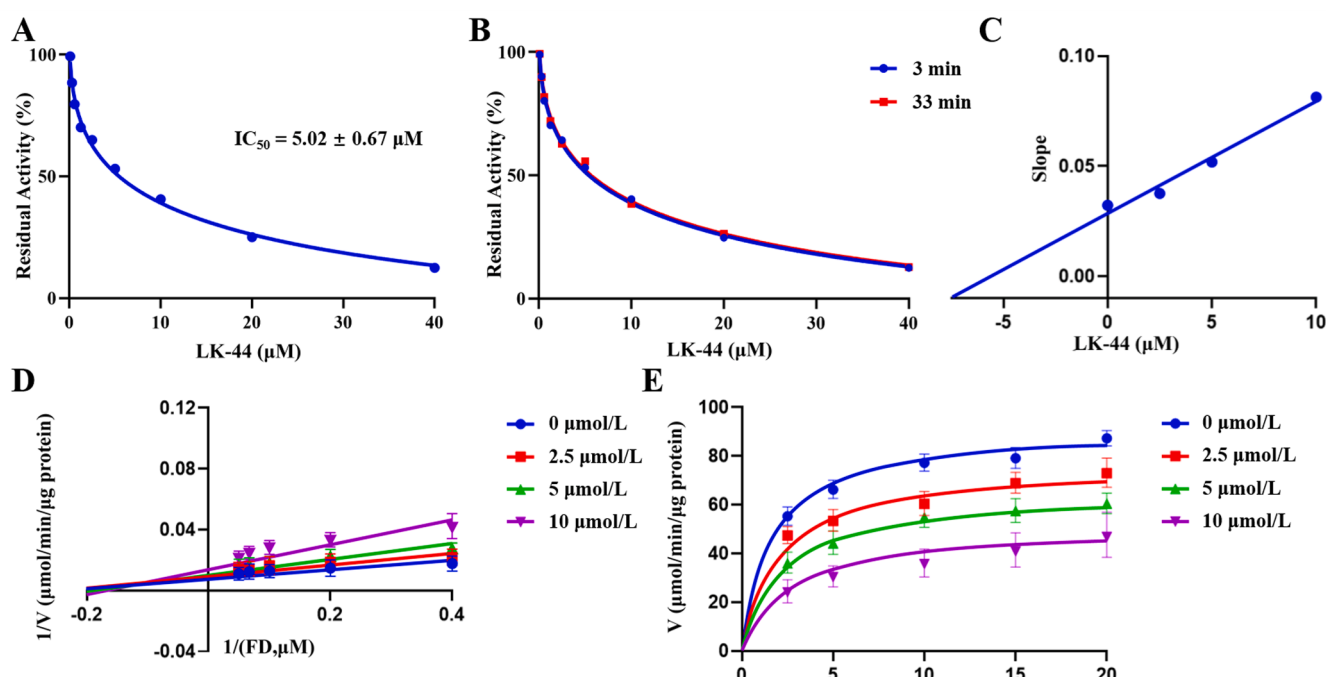


Fig. 4. The inhibitory activities and inhibition kinetics of LK-44 on hCES2A. (A) LK-44 dose-dependent curve of hCES2A-mediated FD hydrolysis; (B) Residual activity of LK-44 for hCES2A-mediated FD hydrolysis at different incubation times; (C) Lineweaver-Burk corresponding Slope plots; (D) The Lineweaver-Burk plot of LK-44 hCES2A-mediated FD hydrolysis; (E) The inhibition kinetics plots of hCES2A-mediated FD hydrolysis by LK-44. All data are expressed as mean ± SD.

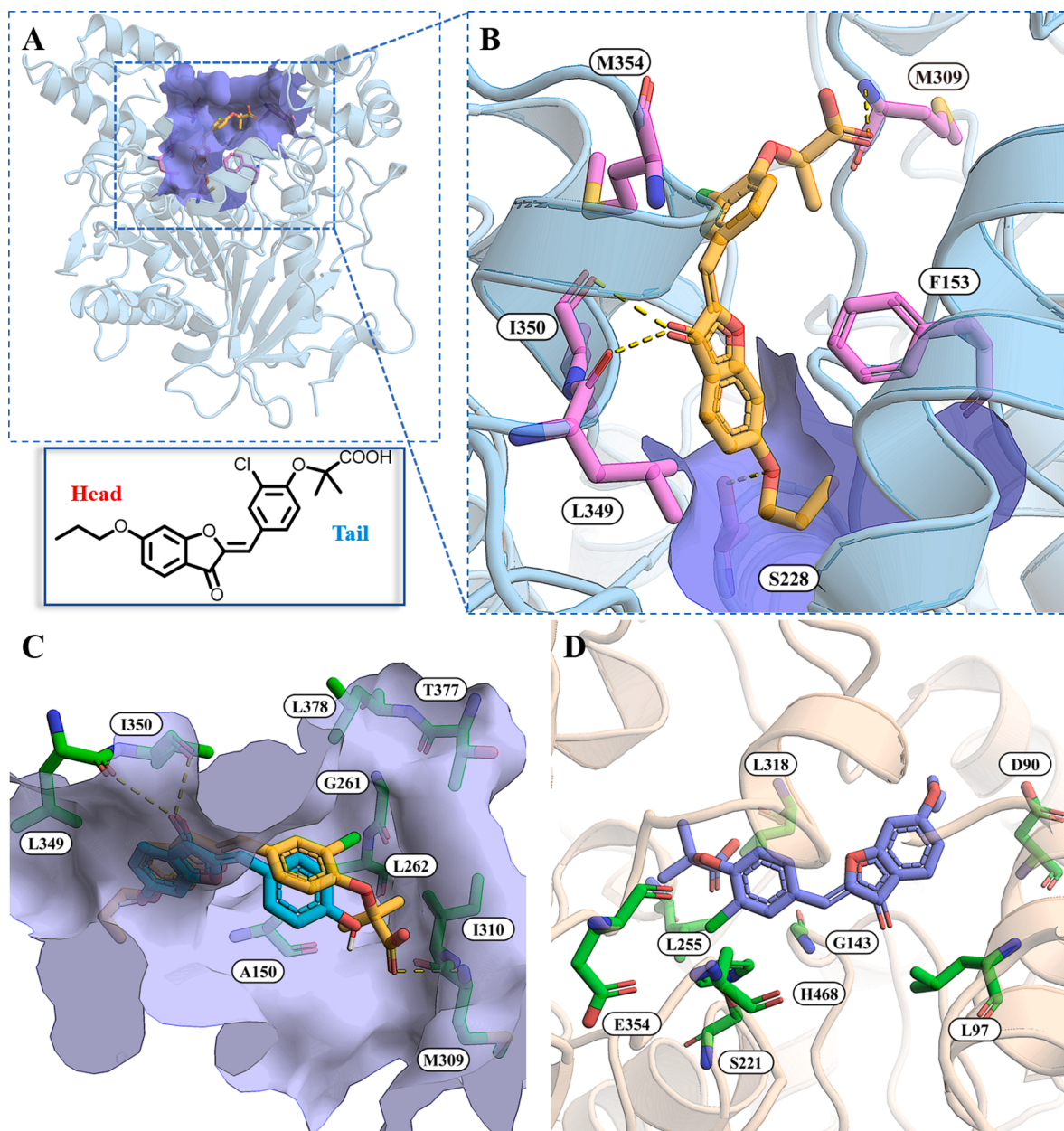


Fig. 5. The docking study of LK-44. (A) Panoramic view of the docking results of LK-44 and hCES2A; (B) Diagram of interaction between LK-44 and hCES2A; (C) Fusion diagram of the docking results of lead compound 01 and LK-44; (D) Diagram of interaction between LK-44 and hCES1A.

4. Experimental section

4.1. General chemistry

The reagents and solvents used in this study were purchased from commercial sources (Shanghai BIDE Medical Technology Co., Ltd, Shanghai, China) and used without further purification. D-luciferin methyl ester (DME) and D-luciferin were purchased from AAT Bioquest (USA). 3-(4,5-dimethylthiazol)-2-, 5-diphenyltetrazolium bromide (MTT) was purchased from Sigma (St. Louis, MO, USA). Irinotecan and loperamide (LPA) were purchased from Shanghai Aladdin Biochemical Technology Co., Ltd. (Shanghai, China). Fluorescein diacetate (FD) was ordered from Shanghai Macklin Biochemical Co., Ltd. (Shanghai, China). Human liver microsomes (HLMs) were obtained from Beijing Huizhi Heyuan Biotechnology Co., Ltd. (Beijing, China). Chromatographic purification was performed on silica gel (200–300 mesh) and the reaction process was analyzed by TLC at 254 and 365 nm using GF254

plates. The melting point was determined by RY-1 apparatus. The Bruker ACF-300Q instrument was used to measure NMR spectra (^1H NMR at 300 MHz or 400 MHz, ^{13}C NMR at 101 MHz) with coupling constants (J values) expressed in Hertz (Hz), and chemical shifts expressed in parts per million (ppm) relative to the internal standard (tetramethylsilane). Mass spectrum data were obtained on a SCIEX X500R QTOF spectrometer equipped with an electrospray ionization (ESI) probe.

4.2. Docking study

The structure of hCES1A was obtained from the Protein Data Bank (<https://www.rcsb.org/>), with the PDB code 1MX1. However, the crystal structure of hCES2A has not yet been resolved, so homology modeling was used to construct the 3D structure of hCES2A based on the reported crystal structure of hCES1A (PDB ID: 1MX1). To accomplish this, the amino acid sequence of hCES2A was retrieved from the UniProt database (Entry code O00748). The 3D structure modeling of hCES2A

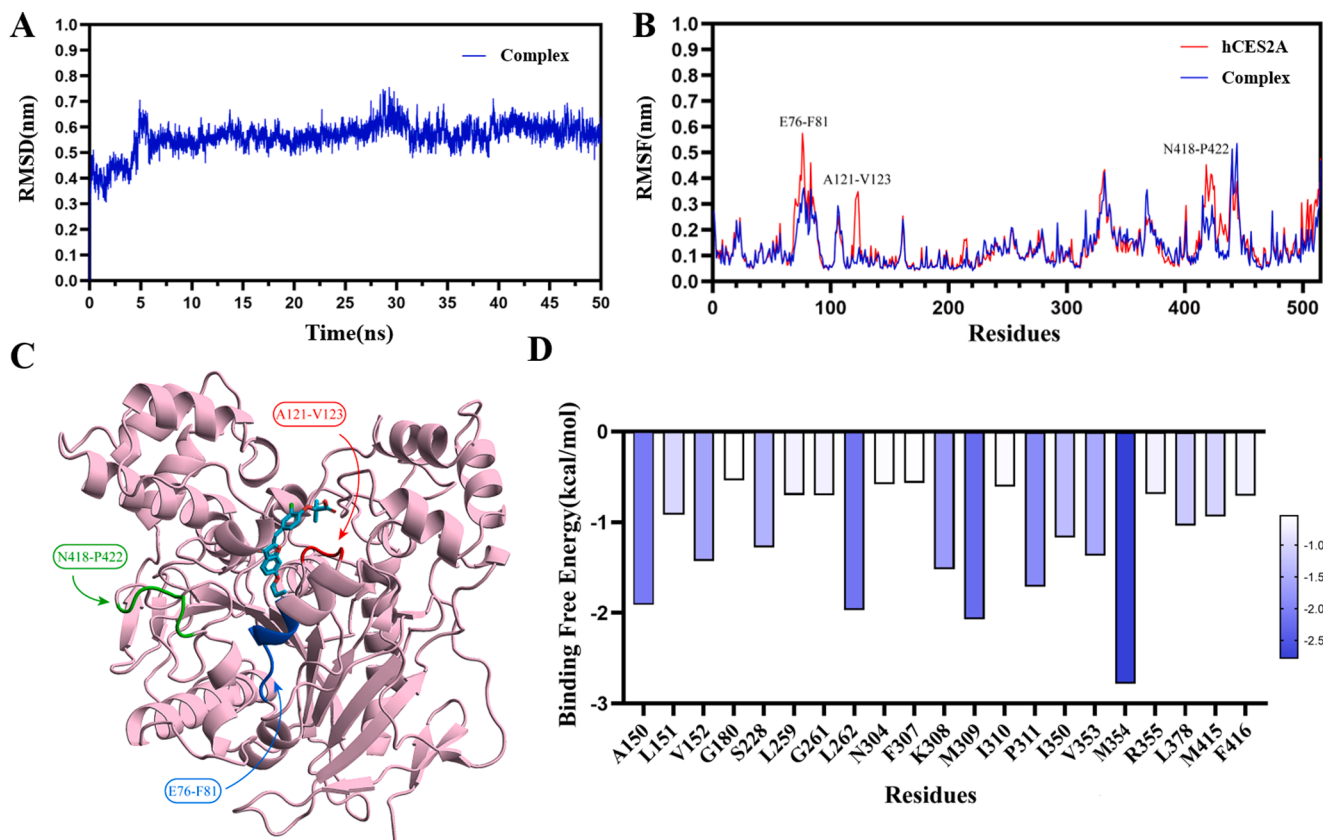


Fig. 6. Molecular dynamics of LK-44 with residues in the active pocket of hCES2A. (A) RMSD change profiles of the complex and free protein systems over 50 ns dynamic simulation; (B) RMSF values of binding site residues in the free protein (red line) and complex systems (blue line); (C) The structure of hCES2A, the regions with high flexibility were displayed in blue (E76-F81), red (A121-V123) and green (N418-P422); (D) Binding free energy decomposition during the molecular dynamic simulation of hCES2A complexed with LK-44. (For interpretation of the references to colour in this figure legend, the reader is referred to the web version of this article.)

was performed using the Swissmodel Automatic Modeling Mode (<https://swissmodel.expasy.org/>), with the resolved structure of hCES1A (PDB ID: 1MX1) serving as an appropriate template due to its 2.4 Å resolution and 48.01% identity. The Global Model Quality Estimation (GMQE) value of the resulting model was 0.77. To evaluate the quality of the hCES2A 3D structure, the Protein Structure and Model Assessment Tools available at the SWISS-MODEL Workspace were utilized. And the QMEAN scoring function of the value was -2.25.

To investigate the binding modes of interaction between a drug candidate and its target, the protein–ligand docking software Autodock Vina 1.1.2 was used. The structure of hCES1A was obtained from the PDB database, while the 3D structure of hCES2A was obtained via homology modeling, as previously described. Before docking study, the protein was added polar hydrogen and gasteiger charger, removed water, and assigned atoms as AD4 based on AutoDock Tools. The MM2 function of ChemBio3D Ultra 14.0 was used for energy optimization of the 3D structure of lead compound 01 and LK-44. Docking was operated using full flexibility of ligand, binding pocket parameters were set (center of x, y, z was 88.9, 85.9, 26.0; size of x, y, z was 46.1, 38.0, 35.1) and kept other parameters as default values. Afterwards, we processed the primary ligand tacrine using the same method as described above and performed a redocking study with the same parameters. The RMSD (root-mean-square-deviation) between the docked tacrine and the crystal structure (1MX1) was calculated using VMD1.9.3 and found to be 1.334. Generally, an RMSD value less than 2 is considered indicative of a relatively reliable docking method. Finally, the molecular docking diagrams were edited and exported using Pymol 2.3.1 (Education Edition).

4.3. The hCES2A inhibition assay

After incubating a mixture of human liver microsomes (HLM, 2 µg/mL final concentration), PBS (0.1 M) buffer, and tested compounds for 10 min at 37 °C, a fluorescent probe substrate FD (15 µM, Macklin Shanghai) was added, and the incubation was prolonged for an additional 20 min at 37 °C. The reaction was then halted by adding an equal volume of ice-cold acetonitrile and vigorously shaking the solution. After centrifuging the reaction at 20,000 RPM and 4 °C for 20 min, the protein was removed, and 200 µL of the supernatant was collected in a 96-well plate. The absorbance of each well (Ex = 480 nm, Em = 520 nm) was measured using a fluorescence micropore apparatus (Thermo, USA). The experimental data for enzyme activity inhibition were obtained from replicates of three independent experiments, and the results for inhibition activity were presented as mean ± standard deviation (SD) [28].

4.4. The hCES1A inhibition assay

After incubating a mixture of human liver microsomes (HLM, 10 µg/mL final concentration), PBS (0.1 M) buffer, and LK-44 for 10 min at 37 °C, a fluorescent probe substrate DME (3 µM, final concentration) was added, and the incubation was prolonged for an additional 10 min at 37 °C. To terminate the reaction, 50 µL of the reaction solution was added to an equal volume of fluorescein detection reagent (Promega USA). The absorbance of each well was then measured at Ex = 600 nm and Em = 662 nm. The experimental data for enzyme activity inhibition were obtained from replicates of three independent experiments, and the results for inhibition activity were presented as mean ± standard

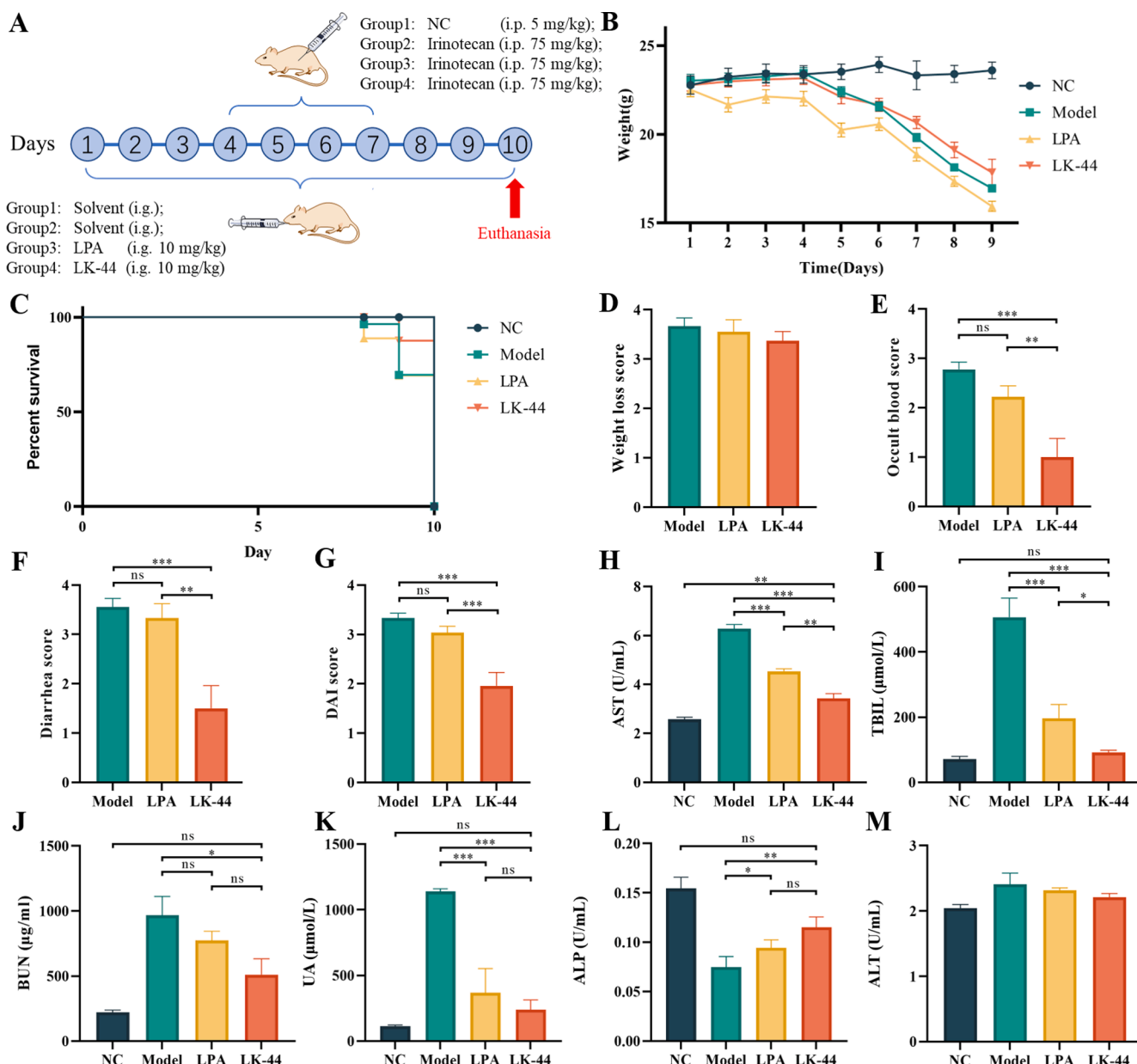


Fig. 7. The effects of LK-44 on Disease Activity Index and Hematological Indexes in the irinotecan-induced delayed diarrhea model. (A) Overview of irinotecan-induced delayed diarrhea model; (B) Weight changes; (C) Survival curve; (D) The weight loss score of mice at 24 h after modeling was compared with that before modeling; (E) The occult blood score of mice at 24 h after modeling; (F) Diarrhea score of mice at 24 h after modeling; (G) Disease Activity Index (DAI) score of mice at 24 h after modeling; (H) Glutamic-Oxalacetic Transaminase (AST); (I) Total bilirubin (TBIL); (J) Urea nitrogen (BUN); (K) Uric acid (UA); (L) Alkaline phosphatase (ALP); (M) Glutamic-Pyruvic Transaminase (ALT); The results were expressed as Mean \pm SD, n = 10 (NC group = 6); *P < 0.05, **P < 0.01, ***P < 0.001 were analyzed using a one-way ANOVA with Tukey's multiple-comparison post hoc test.

deviation (SD) [29,30].

4.5. Inhibition kinetic analyses

In order to determine the type of inhibition kinetics exhibited by LK-44, the inhibition constant values were measured by varying concentrations of FD in the presence or absence of LK-44, using the same culture conditions as in the previous hCES2A inhibition assay. Subsequently, reaction rates were determined using different concentrations of FD and different concentrations of LK-44. The resulting data was analyzed using Dixon plots and Lineweaver-Burk plots, with the intersection of these plots being used to determine the type of inhibition kinetics. Additionally, the slope of the Lineweaver-Burk plot against the inhibitor concentration was used to calculate each inhibition constant

(K_i) value [31,32].

4.6. Molecular dynamics simulations

To perform MD (molecular dynamics) simulations, we utilized the GROMACS 2019.6 [33] software package and the Charmm36 force field to simulate the interaction between LK-44 and hCES2A [34]. The optimal ligand conformation generated by previous molecular docking was used as the initial structure for the MD simulations. The CGenFF Web server (<https://cgenff.umaryland.edu/>) was employed to generate the topology file for the ligand. For the simulation setup, periodic boundary conditions were applied, and each system was immersed in a cubic box of TIP3P water model. A solvent environment containing 0.145 M NaCl and net charge was simulated [35]. To ensure a sufficient

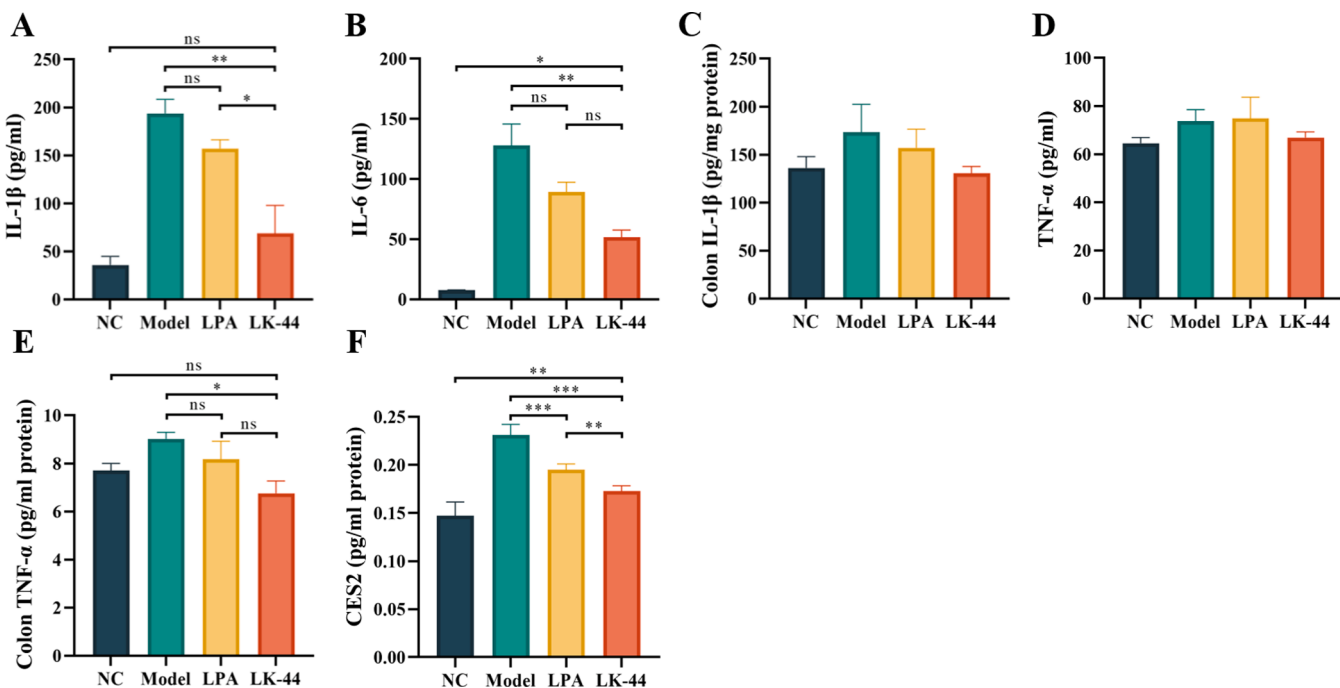


Fig. 8. Assessment of the anti-inflammatory effects of LK-44 in the irinotecan-induced delayed diarrhea model. (A) Serum interleukin-1 beta (IL-1 β); (B) Serum interleukin-6 (IL-6); (C) Colon IL-1 β ; (D) Serum tumor necrosis factor- α (TNF- α); (E) Colon TNF- α ; (F) Colon CES2. The results were expressed as Mean \pm SD, n = 10 (NC group = 6); *P < 0.05, **P < 0.01, ***P < 0.001 were analyzed using a one-way ANOVA with Tukey's multiple-comparison post hoc test.

distance between the ligand and the edge of the simulation box, a minimum distance of at least 12 Å was maintained. Prior to the MD simulations, each system was minimized using the steepest descent algorithm. Additionally, each system was gradually heated from 0 to 310 K over 100 ps under NVT conditions, followed by equilibration at 310 K for 1000 ps under NPT conditions. Finally, each system was simulated for 50 ns with results stored for every 2 fs [36]. For comparative analysis, additional MD simulations were performed on hCES2A under the same parameters.

4.7. Binding free energy calculation

The binding free energy (ΔG_{bind}) of the protein-ligand complex was estimated using the equilibrium part of the trajectory by using the MM/PBSA method [37]. Equilibrium snapshots were taken at 500 ps intervals for calculations. The free energy changes between the two states of the receptor and ligand, the bound state and the free state were calculated according to Equation (1), and each term was defined as equation (2). The molecular mechanical free energy was defined as ΔG_{gas} and was constructed from the electrostatic (ΔG_{ele}) and van der Waals interactions (ΔG_{vdW}) shown in Equation (3). The solvation free energy was composed of polar contributions ($\Delta G_{pol, sol}$) and nonpolar contributions ($\Delta G_{nonpol, sol}$) shown in Equation (4). The polar part was calculated by solving the Poisson-Boltzmann (PB) equation of the MM/PBSA method. According to Equation (5), the solvent accessible surface area (SASA, Å²) and the Amber molsurf module were used to calculate the non-polar part of the solvation free energy, with γ representing the surface tension and set to 0.0072 kcal/mol·Å². And the constant "b" was set to zero. The conformational entropy was expressed as TΔS and can be calculated using the normal method.

$$\Delta G_{bind} = G_{compound} - [G_{protein} + G_{ligand}] \quad (1)$$

$$\Delta G = \Delta_{gas} + \Delta G_{sol} - T\Delta S \quad (2)$$

$$\Delta G_{MM} = \Delta G_{ele} + \Delta G_{vdW} \quad (3)$$

$$\Delta G_{sol} = \Delta G_{pol,sol} + \Delta G_{nonpol,sol} \quad (4)$$

$$\Delta G_{nonpol,sol} = \gamma SASA + b \quad (5)$$

To further investigate the key residues of protein binding to ligands, the contribution of residues in the pocket to ligand binding was estimated using binding free energy decomposition analysis. This decomposition was performed only for molecular mechanics and solvation energies but not for the entropies. The binding free energy was decomposed into the contribution of protein-ligand interaction pairs and consists of four terms: ΔG_{ele} , ΔG_{vdW} , $\Delta G_{pol, sol}$ and $\Delta G_{nonpol, sol}$. The same snapshots adopted for the binding free energy calculations were used for the energy decomposition analysis [38].

4.8. Animals

Male C57BL/6 mice, eight weeks old, were purchased from Guangdong Medical Laboratory Animal Center (Guangdong, China) for the animal experiments. All animal procedures were conducted at the Animal Experiment Center of Guangdong Pharmaceutical University and provided with adequate food and water. The mice were housed in a chamber under a constant 12-hour day-night cycle, with a temperature maintained at 23 to 25 °C and relative humidity kept at 70 ± 10%. All animal experimental protocols were approved by the Ethics Committee of Guangdong Pharmaceutical University and were conducted in accordance with the Laboratory Animal Management Regulations in China. Additionally, the experiments adhered to the Guide for the Care and Use of Laboratory Animals published by the National Institutes of Health (NIH Publication NO. 85-23, revised 2011) to ensure the ethical and humane treatment of the animals.

4.9. Delayed diarrhea experiments

All mice were randomly assigned to one of four groups based on their body weight: NC group (n = 6), Model group (n = 10), LPA group (n = 10), and LK-44 group (n = 10). During the experiment, the diet and

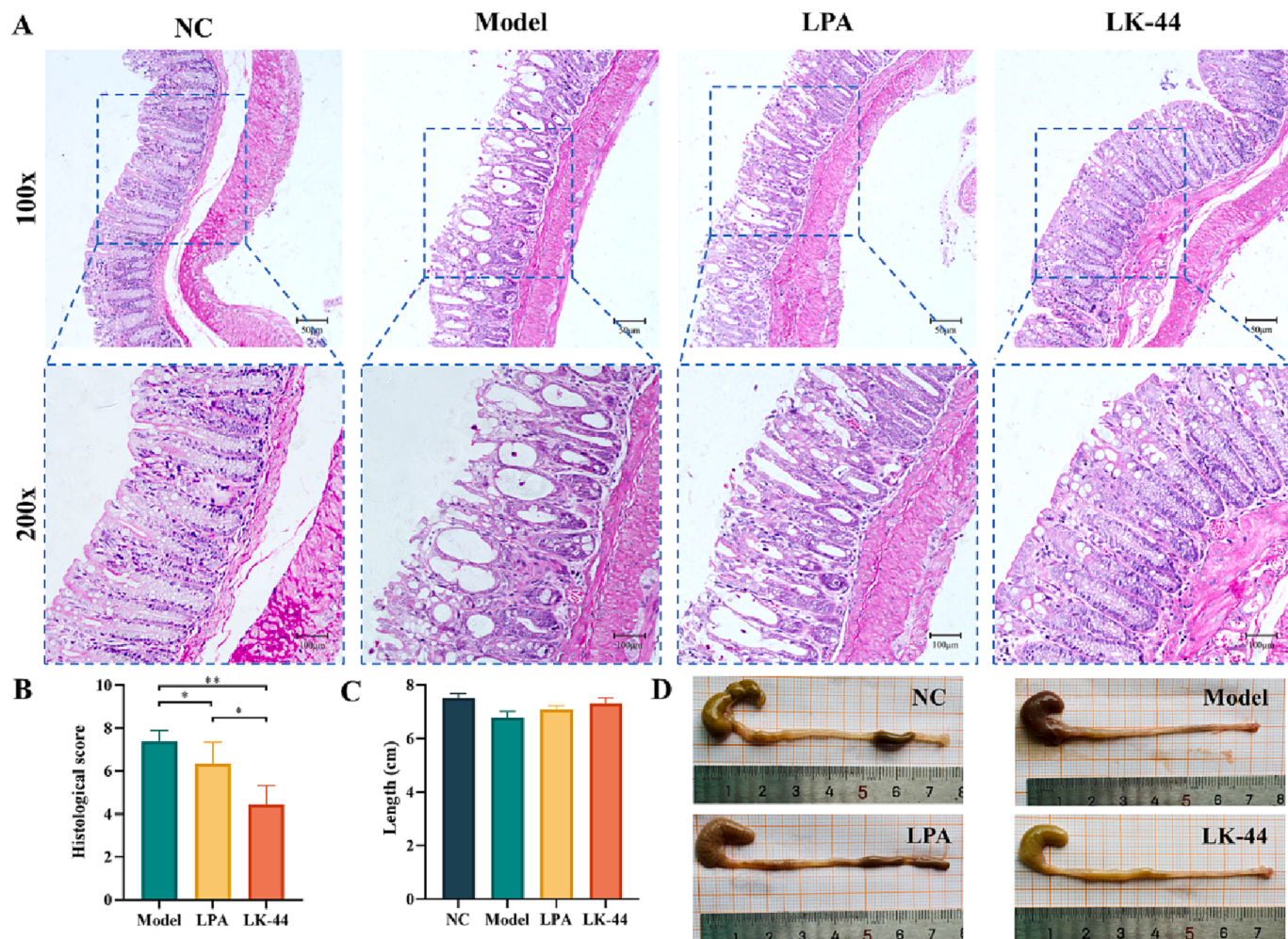


Fig. 9. The effect of LK-44 on histopathology in the irinotecan-induced delayed diarrhea model. (A) Colon sections by H&E staining, scale bars: 50 μ m and 100 μ m; (B) Histological score of H&E staining of colon sections; (C) Colon length of mice in each administration groups; (D) Colon of mice in different administration groups. The results were expressed as Mean \pm SD, n = 10 (NC group = 6); *P < 0.05, **P < 0.01 were analyzed using a one-way ANOVA with Tukey's multiple-comparison post hoc test.

water intake of mice were recorded daily, and the animal morphology was observed. Photographs were taken to record perianal conditions. The mice were orally administered the designated treatment for 10 days. From days 4 to 7, the NC group received intraperitoneal injections of 5 mL/kg 0.9% normal saline, while the other groups were injected with 75 mg/kg irinotecan intraperitoneally 1 h after administration. A mouse model of delayed diarrhea induced by irinotecan was established by continuous injection of irinotecan for 4 days [39]. The DAI measure used in this study is a composite score that takes into account weight loss, diarrhea, and hematochezia as indicators of disease severity. The score is calculated 24 h after the end of irinotecan treatment and is based on the severity of each of these three components (Table S1) [40]. The colon tissues were collected on day 10 of the experiment and subjected to histopathological examination to assess tissue integrity. The histopathological examination involved H&E staining of paraffin-embedded tissues, followed by scoring according to a predefined system. These assessments were used to evaluate the efficacy of LPA and LK-44 in mitigating the symptoms of delayed diarrhea induced by irinotecan (Table S2) [41].

The blood was centrifuged at 5000 \times g for 10 min and the upper serum was collected for biochemical tests. The levels of ALP, ALT, AST, BUN, UA, and TBIL in the serum were measured using the kit instructions (Solarbio, Beijing). The levels of IL-6, IL-1 β , TNF- α , and hCES2A in the colon tissue or serum were detected using ELISA kits and following the

instructions (Multi Sciences, China).

4.10. Statistical analysis

All experiments in this study were performed in triplicate, and the results presented here are all based on the mean \pm SD. The IC₅₀ values and K_i values were calculated using GraphPad Prism 9.0 software.

Declaration of Competing Interest

The authors declare that they have no known competing financial interests or personal relationships that could have appeared to influence the work reported in this paper.

Data availability

Data will be made available on request.

Acknowledgments

This study was supported by Basic and Applied Basic Research of Guangzhou (202201010436), National Key Clinical Specialty Construction Project (Clinical Pharmacy), and High-Level Clinical Key Specialty (Clinical Pharmacy) in Guangdong Province, the Open Project

of Guangxi Key Laboratory of Precision Medicine in Cardio-cerebrovascular Diseases Control and Prevention (GXXNXG202101).

References

- [1] T. Satoh, M. Hosokawa, The mammalian carboxylesterases: from molecules to functions, *Annu. Rev. Pharmacol. Toxicol.* 38 (1998) 257–288.
- [2] M.R. Redinbo, P.M. Potter, Mammalian carboxylesterases: from drug targets to protein therapeutics, *Drug Discov. Today* 10 (5) (2005) 313.
- [3] S. Bencharit, C.C. Edwards, C.L. Morton, E.L. Howard-Williams, P. Kuhn, P. M. Potter, M.R. Redinbo, Multisite promiscuity in the processing of endogenous substrates by human carboxylesterase 1, *J. Mol. Biol.* 363 (1) (2006) 201–214.
- [4] T. Satoh, M. Hosokawa, Carboxylesterases: structure, function and polymorphism in mammals, *J. Pestic. Sci.* 35 (3) (2010) 218–228.
- [5] J.A. Crow, A. Borazjani, P.M. Potter, M.K. Ross, Hydrolysis of pyrethroids by human and rat tissues: examination of intestinal, liver and serum carboxylesterases, *Toxicol. Appl. Pharmacol.* 221 (1) (2007) 1–12.
- [6] M.K. Ross, J.A. Crow, Human Carboxylesterases and their role in xenobiotic and endobiotic metabolism, *J. Biochem. Mol. Toxicol.* 21 (4) (2007) 187–196.
- [7] M. Hosokawa, Structure and catalytic properties of carboxylesterase isozymes involved in metabolic activation of prodrugs, *Molecules* 13 (2) (2008) 412–431.
- [8] T. Imai, M. Taketani, M. Shii, M. Hosokawa, K. Chiba, Substrate specificity of carboxylesterase isozymes and their contribution to hydrolase activity in human liver and small intestine, *Drug Metab. Dispos.* 34 (10) (2006) 1734–1741.
- [9] H.J. Zhu, X.W. Wang, B.E. Grawronski, B.J. Brinda, D.J. Angiollo, J.S. Markowitz, Carboxylesterase 1 as a determinant of clopidogrel metabolism and activation, *J. Pharmacol. Exp. Ther.* 344 (3) (2013) 665–672.
- [10] S.P. Sanghani, S.K. Quinney, T.B. Fredenburg, Z.J. Sun, W.I. Davis, D.J. Murry, O. W. Cummings, D.E. Seitz, W.F. Bosron, Carboxylesterases expressed in human colon tumor tissue and their role in CPT-11 hydrolysis, *Clin. Cancer Res.* 9 (13) (2003) 4983–4991.
- [11] Y. Kobayashi, T. Fukami, M. Shimizu, M. Nakajima, T. Yokoi, Contributions of arylacetamide deacetylase and carboxylesterase 2 to flutamide hydrolysis in human liver, *Drug Metab. Dispos.* 40 (6) (2012) 1080–1084.
- [12] E.T. Williams, K.O. Jones, G.D. Ponsler, S.M. Lowery, E.J. Perkins, S.A. Wrighton, K.J. Ruterborries, M. Kazui, N.A. Farid, The biotransformation of prasugrel, a new thienopyridine prodrug, by the human carboxylesterases 1 and 2, *Drug Metab. Dispos.* 36 (7) (2008) 1227–1232.
- [13] V.A. de Souza, D.J. Scott, J.E. Nettleship, N. Rahman, M.H. Charlton, M.A. Walsh, R.J. Owens, Comparison of the structure and activity of glycosylated and aglycosylated human carboxylesterase 1, *PLoS One* 10 (12) (2015) 12.
- [14] S. Bencharit, C.L. Morton, Y. Xue, P.M. Potter, M.R. Redinbo, Structural basis of heroin and cocaine metabolism by a promiscuous human drug-processing enzyme, *Nat. Struct. Biol.* 10 (5) (2003) 349–356.
- [15] M.K. Ma, H.L. McLeod, Lessons learned from the irinotecan metabolic pathway, *Curr. Med. Chem.* 10 (1) (2003) 41–49.
- [16] R.Z. Hahn, M.V. Antunes, S.G. Verza, M.S. Perassolo, E.S. Suyenaga, G. Schwartsmann, R. Linden, Pharmacokinetic and pharmacogenetic markers of irinotecan toxicity, *Curr. Med. Chem.* 26 (12) (2019) 2085–2107.
- [17] M. Kciuk, B. Marciniaik, R. Kontek, Irinotecan-still an important player in cancer chemotherapy: a comprehensive overview, *Int. J. Mol. Sci.* 21 (14) (2020) 21.
- [18] H. Miller, L. Panahi, D. Tapia, A. Tran, J.D. Bowman, Loperamide misuse and abuse, *J. Am. Pharm. Assoc.* 57 (2) (2017) S45–S50.
- [19] Y.J. Liu, S.Y. Li, J. Hou, Y.F. Liu, D.D. Wang, Y.S. Jiang, G.B. Ge, X.M. Liang, L. Yang, Identification and characterization of naturally occurring inhibitors against human carboxylesterase 2 in White Mulberry Root-bark, *Fitoterapia* 115 (2016) 57–63.
- [20] Z.P. Mai, K. Zhou, G.B. Ge, C. Wang, X.K. Huo, P.P. Dong, S. Deng, B.J. Zhang, H. L. Zhang, S.S. Huang, X.C. Ma, Prostostane triterpenoids from the rhizome of alisma orientale exhibit inhibitory effects on human carboxylesterase 2, *J. Nat. Prod.* 78 (10) (2015) 2372–2380.
- [21] E.I. Parkinson, M.J. Hatfield, L. Tsurkan, J.L. Hyatt, C.C. Edwards, L.D. Hicks, B. Yan, P.M. Potter, Requirements for mammalian carboxylesterase inhibition by substituted ethane-1,2-diones, *Bioorg. Med. Chem.* 19 (15) (2011) 4635–4643.
- [22] R.M. Wadkins, J.L. Hyatt, C.C. Edwards, L. Tsurkan, M.R. Redinbo, C.E. Wheelock, P.D. Jones, B.D. Hammock, P.M. Potter, Analysis of mammalian carboxylesterase inhibition by trifluoromethylketone-containing compounds, *Mol. Pharmacol.* 71 (3) (2007) 713–723.
- [23] Y.Q. Song, Q. Jin, D.D. Wang, J. Hou, L.W. Zou, G.B. Ge, Carboxylesterase inhibitors from clinically available medicines and their impact on drug metabolism, *Chem. Biol. Interact.* 345 (2021) 20.
- [24] P.C. Huo, X.Q. Guan, P. Liu, Y.Q. Song, M.R. Sun, R.J. He, L.W. Zou, L.J. Xue, J. H. Shi, N. Zhang, Z.G. Liu, G.B. Ge, Design, synthesis and biological evaluation of indanone-chalcone hybrids as potent and selective hCES2A inhibitors, *Eur. J. Med. Chem.* 209 (2021) 10.
- [25] K.W. Bock, Roles of human UDP-glucuronosyltransferases in clearance and homeostasis of endogenous substrates, and functional implications, *Biochem. Pharmacol.* 96 (2) (2015) 77–82.
- [26] S. Oda, T. Fukami, T. Yokoi, M. Nakajima, A comprehensive review of UDP-glucuronosyltransferase and esterases for drug development, *Drug Metab. Pharmacokinet.* 30 (1) (2015) 30–51.
- [27] D.D. Wang, Q. Jin, L.W. Zou, J. Hou, X. Lv, W. Lei, H.L. Cheng, G.B. Ge, L. Yang, A bioluminescent sensor for highly selective and sensitive detection of human carboxylesterase 1 in complex biological samples, *Chem. Commun.* 52 (15) (2016) 3183–3186.
- [28] Y.Q. Song, X.Q. Guan, Z.M. Weng, Y.Q. Wang, J. Chen, Q. Jin, S.Q. Fang, B. Fan, Y. F. Cao, J. Hou, G.B. Ge, Discovery of a highly specific and efficacious inhibitor of human carboxylesterase 2 by large-scale screening, *Int. J. Biol. Macromol.* 137 (2019) 261–269.
- [29] P.F. Song, Y.D. Zhu, H.Y. Ma, Y.N. Wang, D.D. Wang, L.W. Zou, G.B. Ge, L. Yang, Discovery of natural pentacyclic triterpenoids as potent and selective inhibitors against human carboxylesterase 1, *Fitoterapia* 137 (2019) 7.
- [30] J. Zhang, Q.S. Pan, X.K. Qian, X.L. Zhou, Y.J. Wang, R.J. He, L.T. Wang, Y.R. Li, H. Huo, C.G. Sun, L. Sun, L.W. Zou, L. Yang, Discovery of triterpenoids as potent dual inhibitors of pancreatic lipase and human carboxylesterase 1, *J. Enzym. Inhib. Med. Chem.* 37 (1) (2022) 629–640.
- [31] Y.Z. Liu, L.H. Pan, Y. Bai, K. Yang, P.P. Dong, Z.Z. Fang, Per- and polyfluoroalkyl substances exert strong inhibition towards human carboxylesterases, *Environ. Pollut.* 263 (2020) 9.
- [32] L.M.S. Nobre, M.H.D. Lopes, J. Geraix, A.G. Cajado, J.M.R. Silva, L.R. Ribeiro, R. S. Freire, D.I.M. Cavalcante, D.V.T. Wong, A. Alves, R.C.P. Lima, Paraprobiotic *Enterococcus faecalis* EC-12 prevents the development of irinotecan-induced intestinal mucositis in mice, *Life Sci.* 296 (2022) 13.
- [33] D. Van der Spoel, E. Lindahl, B. Hess, G. Groenhof, A.E. Mark, H.J.C. Berendsen, GROMACS: fast, flexible, and free, *J. Comput. Chem.* 26 (16) (2005) 1701–1718.
- [34] O. Guvench, S.S. Mallajosyula, E.P. Raman, E. Hatcher, K. Vanommeslaeghe, T. J. Foster, F.W. Jamison, A.D. MacKerell, CHARMM additive all-atom force field for carbohydrate derivatives and its utility in polysaccharide and carbohydrate-protein modeling, *J. Chem. Theory Comput.* 7 (10) (2011) 3162–3180.
- [35] P. Mark, L. Nilsson, Structure and dynamics of the TIP3P, SPC, and SPC/E water models at 298 K, *J. Phys. Chem. A* 105 (43) (2001) 9954–9960.
- [36] Y. Ma, H.L. Li, X.B. Chen, W.Y. Jin, H. Zhou, Y. Ma, R.L. Wang, 3D QSAR pharmacophore based virtual screening for identification of potential inhibitors for CDC25B, *Comput. Biol. Chem.* 73 (2018) 1–12.
- [37] B.R. Miller, T.D. McGee, J.M. Swails, N. Homeyer, H. Gohlke, A.E. Roitberg, MMPBSA.py: an efficient program for end-state free energy calculations, *J. Chem. Theory Comput.* 8 (9) (2012) 3314–3321.
- [38] H. Gohlke, C. Kiel, D.A. Case, Insights into protein-protein binding by binding free energy calculation and free energy decomposition for the Ras-Raf and Ras-RalGDS complexes, *J. Mol. Biol.* 330 (4) (2003) 891–913.
- [39] S.J. Yue, Y.F. Qin, A. Kang, H.J. Tao, G.S. Zhou, Y.Y. Chen, J.Q. Jiang, Y.P. Tang, J. A. Duan, Total flavonoids of *Glycyrrhiza uralensis* alleviates irinotecan-induced colitis via modification of Gut microbiota and fecal metabolism, *Front. Immunol.* 12 (2021) 13.
- [40] X.X. Wei, Y. Yang, M. Liu, A. Luo, H. Song, Y. Wang, X. Duan, New discovery of antiulcerative colitis active ingredients of *Nostoc commune*: p-Hydroxy benzaldehyde, *J. Funct. Foods* 77 (2021) 13.
- [41] B. Katsandegwaza, W. Horanell, K. Smith, Inflammatory bowel disease: a review of pre-clinical murine models of human disease, *Int. J. Mol. Sci.* 23 (2022) 16.